

Cite this: *J. Mater. Chem. B*, 2023, **11**, 359

Electrospun flexible magnesium-doped silica bioactive glass nanofiber membranes with anti-inflammatory and pro-angiogenic effects for infected wounds†

Mingyue Liu,^{‡a} Xiangsheng Wang,^{‡b} Jie Cui,^a Hongsheng Wang,^a Binbin Sun,^a Jufang Zhang,^b Bernd Rolaufts,^c Muhammad Shafiq,^{id a} Xiumei Mo,^{id *a} Zhanyong Zhu^{*d} and Jinglei Wu^{id *a}

Antibacterial, anti-inflammatory, and pro-angiogenic properties are prerequisites for dressing materials that accelerate the healing process of infected wounds. Herein, we report a magnesium-doped silica bioactive glass (SiO₂/MgO) nanofiber membrane prepared by electrospinning. Our results demonstrate that this SiO₂/MgO nanofiber membrane has good flexibility and hydrophilicity, which give it intimate contact with wound beds. *In vitro* assessments illustrate its good cytocompatibility and bioactivity that contribute to its robust cell proliferation and angiogenesis. It shows capacity in modulating the cellular inflammatory response of murine macrophages. In addition, *in vitro* assays prove its good antibacterial activity against both Gram-positive and Gram-negative strains. In a full-thickness skin defect inoculated with *Staphylococcus aureus* in mice, it effectively inhibits bacterial infection. Both gene expression and histological/immunohistochemical analyses confirmed the down-regulated pro-inflammatory factors, up-regulated anti-inflammatory factors, and enhanced angiogenesis. Taken together, these desirable properties work in concert to contribute to the rapid healing of infected wounds and make it a good candidate for wound dressing materials.

Received 20th September 2022,
Accepted 1st December 2022

DOI: 10.1039/d2tb02002e

rsc.li/materials-b

1. Introduction

Wound infection remains a persistent challenge and poses a huge burden on patients and healthcare systems worldwide.¹ Upon a trauma or an injury, the integrity of the skin is compromised, which is followed by an intrinsic healing response to protect the injured skin.² During the healing process, wounds are vulnerable to external insults such as

mechanical collision or bacterial infection. Dressing materials that shield wound beds, keep in moisture and prevent wounds from external insults are of central importance for robust wound healing. However, bacterial infection is inevitable and greatly affects the wound healing process. Many antibacterial biomaterials, such as nanofiber membranes, injectable hydrogels, inorganic metal oxides, and organic/inorganic composites have been investigated as substitutes to replace traditional dressings (gauze and cotton wool) for treating wounds.^{3–5} Although great progress has been made, there is an ongoing need for novel antibacterial wound dressing materials.

In addition to the antibacterial capacity, good biological activity is another prerequisite for promoting wound healing.^{6,7} Electrospinning is the simplest technique to produce fibrous membranes, by which biological substances could be feasibly incorporated into nanofibers. Recently, we and other research groups reported the incorporation of inorganic nanoparticles (NPs) such as silver,⁸ magnesium oxide (MgO),⁹ zinc oxide (ZnO),¹⁰ and copper-containing bioactive glass¹¹ into polymeric nanofibers for treating infected wounds. For instance, MgO-incorporated electrospun membranes effectively inhibit bacterial infection and modulate inflammatory responses, which gives rise to accelerated wound healing.^{3,9} However, aggregation of MgO

^a State Key Laboratory for Modification of Chemical Fibers and Polymer Materials, Shanghai Engineering Research Center of Nano-Biomaterials and Regenerative Medicine, College of Biological Science and Medical Engineering, Donghua University, Shanghai, 201620, P. R. China. E-mail: jw@dhu.edu.cn, xmm@dhu.edu.cn

^b Department of Plastic Surgery, Affiliated Hangzhou First People's Hospital, Zhejiang University School of Medicine, Hangzhou, Zhejiang, 310006, P. R. China

^c G. E. R. N. Research Center for Tissue Replacement, Regeneration & Neogenesis, Department of Orthopedics and Trauma Surgery, Faculty of Medicine, Medical Center—Albert-Ludwigs-University of Freiburg, 79085, Freiburg im Breisgau, Germany

^d Department of Plastic Surgery, Renmin Hospital of Wuhan University, Wuhan, Hubei, 430060, P. R. China. E-mail: zyzhu@whu.edu.cn

† Electronic supplementary information (ESI) available. See DOI: <https://doi.org/10.1039/d2tb02002e>

‡ These authors contributed equally to this work.

nanoparticles in electrospun nanofibers could result in a burst release of MgO. Overdosing with MgO might be toxic to the body, raising safety concerns and limiting its clinical applicability.

Recently, silicate bioactive materials have gained increasing interest in biomedical applications due to their good pro-angiogenic potential.^{12–17} Bioactive glasses (BGs) stimulate endothelial cell proliferation and promote endothelial tubule formation^{15,16,18} However, these BGs are used in the form of particles, which cause some problems in clinical practice including rapid dissolution, fast degradation, and burst release of inorganic ions. Converting particulate BGs into fibers by electrospinning represents a brilliant approach to circumvent these problems.^{19,20} In contrast to conventional polymeric nanofibers, recent reports have shown that electrospun inorganic silica nanofibers are capable of sustained release of bioactive substances.²¹ Therefore, incorporating metallic oxide-based NPs into silica BG nanofibers might be an attractive strategy for controlled release of inorganic bioactives.

The objective of this study is to develop a flexible SiO₂/MgO nanofiber membrane and evaluate its potential for promoting wound healing in a bacterial-infected wound model of mice. Specifically, flexible SiO₂/MgO nanofiber membranes were fabricated by electrospinning and calcination. The physico-chemical properties of SiO₂/MgO membranes were characterized and their cytocompatibility and bioactivity were evaluated *in vitro*. Antibacterial activity against Gram-positive and Gram-negative strains was assessed by an *in vitro* study. Finally, the SiO₂/MgO membrane was applied in a full-thickness *S. aureus*-infected wound model in mice to evaluate its potential for promoting infected wound healing.

2. Materials and methods

2.1 Materials

Tetraethyl orthosilicate (TEOS, Sigma-Aldrich, Shanghai, China), phosphoric acid (H₃PO₄, Shanghai Lingfeng Chemical reagent Co., Ltd. Shanghai, China), and polyvinyl alcohol (PVA, Mn = 86 kDa, Aladdin Chemicals, Shanghai, China) were used as received without any further purification. Chloramine T, sulfuric acid, hydroxyproline, and magnesium nitrate hexahydrate (Mg(NO₃)₂·6H₂O) were obtained from Shanghai Aladdin Bio-Chem Technology Co., Ltd (Shanghai, China). Lipopolysaccharides (LPS, from *Escherichia coli* O55:B5, Aladdin, Shanghai, China) and interferon-γ (IFN-γ, PeproTech, Rocky Hill, USA) were also purchased. Routine chemicals were of analytical grade and were used as such without any further purification.

2.2 Fabrication of electrospun flexible SiO₂/MgO membranes

Electrospun membranes composed of SiO₂ nanofibers (SiO₂ NF) were fabricated by following our previous report.²¹ On the other hand, electrospun membranes composed of SiO₂/MgO nanofibers were fabricated by sol-gel electrospinning. The precursor solution for electrospinning was a mixture of Si-Mg sol and PVA solution. Firstly, a 10 wt% PVA solution was prepared by dissolving PVA in deionized water and stirring at

80 °C for 8 h. To afford Si-Mg sol, Mg(NO₃)₂·6H₂O and TEOS with Mg/Si weight ratios of 1%, 2%, 3%, and 4% (SiO₂/MgO-1%, SiO₂/MgO-2%, SiO₂/MgO-3%, and SiO₂/MgO-4%, respectively) were dissolved in deionized water/phosphoric acid (1/0.07, v/v) solution and stirred at room temperature for 12 h. Subsequently, PVA solution and Si-Mg sol were mixed with a weight ratio of 1:1 followed by stirring for up to 5 h at room temperature. The preparation was fed at 1 mL h⁻¹ and electrospun at a high voltage of 20 kV and collected by a slow-speed mandrel (60 rpm) at 15 cm to obtain PVA/Si-Mg composite nanofiber membranes. Then, the PVA/Si-Mg nanofibers (PVA/Si-Mg NF) were calcined at 800 °C for 2 h to prepare SiO₂/MgO nanofibers.

2.3 Characterization of electrospun flexible SiO₂/MgO membranes

The surface morphology and chemical composition of electrospun flexible SiO₂/MgO membranes were analyzed using a scanning electron microscope (SEM, Hitachi, TM-1000, Tokyo, Japan) and an ESM spectrometer. Fiber diameters of SiO₂/MgO electrospun membranes were measured from SEM micrographs by using Image J software. The chemical structure and crystalline phase of electrospun SiO₂/MgO membranes were determined by Fourier transform infrared spectroscopy (FTIR) and X-ray diffraction (XRD), respectively. The attenuated total reflection mode of a Nicolet-760 FTIR spectrometer (Thermo Fisher Scientific, USA) was used to collect the wavelength of samples within the range of 3600 cm⁻¹ to 1000 cm⁻¹. For XRD analysis, a Bruker AXS D8 Discover X-ray diffractometer was used to detect the crystalline phase of samples at a 2θ degree between 10° and 60°.

The moisture permeability of electrospun SiO₂/MgO membranes was evaluated by measuring their water vapor transmission rates (WVTRs) as described elsewhere.⁹ Briefly, commercial transparent dressings (control) as well as SiO₂/MgO membranes were cut into discs and mounted on the mouth of a cylindrical cup containing deionized water. The electrospun SiO₂/MgO membranes and commercial transparent dressings were maintained in an incubator at 37 °C with 50% humidity for 24 h. The water uptake ability of electrospun SiO₂/MgO membranes was determined by following a previous report.⁹ Membranes were tailored into 2 cm × 2 cm squares and weighed (W₀). Samples were then immersed in deionized water at room temperature overnight and the surface water was carefully wiped away using filter paper and then the membranes were weighed again (W₁). The water uptake ability of the membranes was calculated using eqn (1):

$$\text{Water uptake ability} = (W_1 - W_0)/W_0 \times 100\% \quad (1)$$

where W₀ and W₁ indicate the weights of membranes before and after incubation (n = 3 for each group). The surface hydrophobicity of electrospun SiO₂/MgO membranes was assessed using a contact angle analyzer (SL200A, Solon Tech., Shanghai, China). A droplet of deionized water (volume, 5 μL) was dropped onto the surface of membranes and the video was recorded until the drop disappeared. Images at intervals of 5 s were extracted from the videos to calculate the water contact angle. A tangent line of the droplet on the sample surface

was made to determine the water contact angle of electrospun SiO₂/MgO membranes ($n = 4$ for each group). To quantitatively assess the *in vitro* degradation, electrospun membranes were weighed (W_0) prior to incubation in PBS. At pre-determined time points, the incubated membranes were removed, lyophilized, and re-weighed (W_t) ($n = 3$ for each group). The degradation rate of membranes was determined by assessing the percentage of the remaining mass and calculated using eqn (2):

$$\text{Percentage of remained mass (\%)} = W_t/W_0 \times 100\% \quad (2)$$

The release of silicon and magnesium ions from electrospun membranes was performed by incubating samples in 0.9% phosphate-buffered saline at 37 °C. At pre-determined time points, the solution was collected for analysis and replaced with an equal volume of the fresh solution. The concentration of silicon and magnesium ions was determined by inductively-coupled plasma atomic emission spectroscopy (ICP-AES) (Prodigy Plus, Leeman, USA) ($n = 4$ for each group). *In vitro* degradation of SiO₂/MgO electrospun membranes was performed by incubating samples in PBS according to our previous study.²¹ Electrospun SiO₂/MgO membranes were tailored into strip specimens (10 × 40 mm) for uniaxial tensile tests. Details of the methods are provided in the ESI.†

2.4 Cytocompatibility and bioactivity of electrospun SiO₂/MgO membranes

Since electrospun membranes directly contact the wound bed after transplantation, we employed key effector cells involved in the healing process, including human foreskin fibroblasts (HFFs), human umbilical vein endothelial cells (HUVECs), and murine macrophages (RAW 264.7 cell line), which were obtained from the Cell Bank of the Chinese Academy of Sciences, Shanghai, China. Cells were maintained and expanded in high glucose DMEM medium supplemented with 10% fetal bovine serum (FBS) and 1% penicillin/streptomycin. Electrospun membranes were disinfected with 70% ethanol for 1 h and then irradiated by using ultraviolet (UV) light for 12 h on each side prior to cell seeding *in vitro*.

HUVECs and HFFs were separately seeded onto the surface of electrospun membranes at a cell density of 10×10^4 cells per disc. Cell-seeded membranes were maintained in an incubator at 37 °C with 95% humidity and 5% CO₂. The medium was refreshed every other day. The viability and proliferation of HUVECs and HFFs on SiO₂/MgO membranes were assessed by live/dead staining and CCK-8 assay ($n = 4$ for each group), respectively. The cell morphology on nanofiber membranes was further observed by SEM. After 4 days of culture, cell-seeded membranes were briefly rinsed with PBS, stained with Calcein-AM and propidium iodide for 30 min at 37 °C, and imaged with a fluorescence microscope (DMI 8, Leica, Germany) ($n = 4$ for each group). For SEM, cell-seeded membranes were washed with PBS, fixed by using 4% paraformaldehyde (PFA), dehydrated with gradient ethanol series, and dried at room temperature. All samples were sputter-coated with gold and observed using a scanning electron microscope (Phenom, Netherlands). The cell

proliferation on electrospun membranes was assessed by CCK-8 assay. Cell-seeded membranes were incubated with a CCK-8 kit (Beyotime Biotechnology, Shanghai, China) at 37 °C for 2 h, and then 100 μL supernatant from each well was collected and the wavelength was recorded at 450 nm using a microplate reader (Multiskan MK3, Thermo Fisher Scientific, USA) ($n = 4$ for each group).

To determine the effect of nanofiber membranes on vascular endothelial growth factor (VEGF) expression, HUVECs were seeded at a density of 3×10^5 cells per well on membranes in 6-well plates. After 7 days of culture, cell culture medium was harvested to measure accumulated VEGF using a VEGF kit (Invitrogen) following the manufacturer's instructions ($n = 4$ for each group). HFFs were seeded at a density of 3×10^5 cells per well on membranes in 6-well plates to assess the amounts of cell-secreted total protein and collagen and transforming growth factor-β1 (TGF-β1). Total protein was determined using a BCA kit (Beyotime Biotechnology, Shanghai) following the manufacturer's instructions ($n = 4$ for each group). Collagen deposition on membranes was measured using a hydroxyproline assay as described in our previous study.³ Accumulation of HFFs produced TGF-β1 on membranes was determined by a TGF-β1 kit (Invitrogen) following the manufacturer's instructions ($n = 4$ for each group).

Murine macrophages were seeded at a density of 5×10^4 cells per well on membranes in 24-well plates to determine cell viability. At day 7, the cell viability and morphology of RAW264.7 macrophages were assessed by live/dead staining and SEM imaging, respectively. To investigate the immunomodulatory effect of SiO₂/MgO membranes on macrophages, an LPS induced assay was performed as described elsewhere.²² Murine macrophages were seeded at densities of 3×10^5 cells per well on membranes in 6-well plates and cultured in complete medium for 24 h, followed by incubating in complete medium containing 100 ng mL⁻¹ of LPS for 24 h. Cell culture medium was harvested and cumulative expression levels of interleukin 6 (IL-6) and tumor necrosis factor-alpha (TNF-α) were determined separately using ELISA kits (Invitrogen) by following the manufacturer's instructions ($n = 4$ for each group).

To investigate the role of electrospun SiO₂/MgO membranes in regulating macrophage polarization in an inflammatory environment, 5×10^5 cells per well were seeded in 6-well plates. After the attachment of macrophages, the culture medium was replaced with either culture medium (control group), culture medium containing 1000 μg mL⁻¹ LPS and 20 ng mL⁻¹ IFN-γ (LPS + IFN-γ group), or pre-prepared membrane-incubated medium containing 1000 μg mL⁻¹ LPS, 20 ng mL⁻¹ IFN-γ (LPS + IFN-γ + SiO₂/MgO-2% group), as described in the ESI.† After incubating the different media for 24 h, the polarization of macrophages to the M1 subpopulation was identified by flow cytometry.

2.5 Antibacterial activity of electrospun SiO₂/MgO membranes

The antibacterial activity of electrospun SiO₂/MgO membranes was assessed against three commonly used bacterial species:

Gram-negative bacteria *Escherichia coli* (*E. coli*, ATCC 25922), Gram-positive bacteria *Staphylococcus aureus* (*S. aureus*, ATCC 25923), and *Staphylococcus epidermidis* (*S. epidermidis*, ATCC 12228). Samples were irradiated under UV light for 12 hours on each side before inoculating bacterial strains. Bacteria were cultivated in Mueller–Hinton broth with shaking at 37 °C overnight. Each sample was inoculated with 100 μL germly inoculum (10^5 CFU mL^{-1}) and incubated at 37 °C overnight. Aliquots of bacterial inoculated membranes were agitated in sterile PBS for 10 min, serially diluted, and spread on Luria–Bertani agar plates. Bacterial colonies were counted after 24 h incubation at 37 °C ($n = 3$ for each group) and the morphology of the bacterial strains was observed by using SEM. In addition, live/dead staining of bacteria was performed using DMAO and EthD-III to show bacterial survival on electrospun SiO_2/MgO membranes and imaged with a fluorescence microscope (DMi 8, Leica, Germany).

2.6 Assessment of *S. aureus*-infected wound healing

In vivo antibacterial properties of electrospun SiO_2/MgO membranes were assessed in an infection model of mice skin wounds. All procedures were performed in accordance with the guidelines approved by the Animal Ethical Committee of Wuhan University. Twenty-four adult C57BL/6 mice (male; age: 8 weeks; weight: 23–26 g) were housed in a laboratory at 22–25 °C and 40–70% humidity at a light-dark cycle of 12 h. All operations were performed under sterile conditions. Mice were anesthetized by inhalation of 2% isoflurane. The dorsal area was shaved, and a depilatory cream was used to completely remove the hair. The skin was disinfected and then full-thickness skin wounds (diameter, 7 mm) were made on the dorsal skin. All mice were divided into four groups: normal wound (control group), *S. aureus* (SA) group, SA + dressing (3M Adhesive Bandages) group, and SA + SiO_2/MgO -2% group. Except for the control group, the other three groups received SA (2.0×10^9 CFU mL^{-1} , 20 μL per mouse, intraslesional injected). After 12 hours, the wound area was treated with different dressings and gross images were recorded at different endpoints. The area of the wounds was calculated and analyzed by tracing around the wound image margins using Image-Pro Plus software version 6.0 (Media Cybernetics, Rockville, MD, USA). Wound closure was expressed as a percentage area of the original wound.

At day 14 postoperative, each wound area was resected from the skin and halved into two pieces. For each wound area, one-half piece was freshly stored in liquid nitrogen for quantitative real-time polymerase chain reaction (qRT-PCR) ($n = 3$ wounds for each group), and the other half piece was rinsed in PBS, fixed in 4% paraformaldehyde, and embedded in paraffin. The samples were then sectioned and stained using hematoxylin-eosin (H&E) and Masson's trichrome staining for histological analyses. For immunobiological staining, paraffin-embedded tissue sections were incubated with rabbit anti-CD31 and anti-CD68 antibodies (Abcam, Cambridge, UK), followed by incubation with a horseradish peroxidase-conjugated secondary antibody (Dako Glostrup, Denmark). To evaluate angiogenesis in

the wound, CD31+ tubular structures were considered to be capillaries and the capillary density in the wound area, undergoing healing, were quantified. To analyze the inflammatory response of the wound, CD68+ macrophages were calculated. The detailed methods are provided in the ESI.†

2.7 Statistical analysis

Data are presented as means \pm standard deviations. All data were analyzed using an unpaired Student's *t*-test or one-way analysis of variance (ANOVA) where appropriate. Statistical significance was considered at $p < 0.05$.

3. Results

3.1 Physiochemical properties of electrospun flexible SiO_2/MgO membranes

We prepared SiO_2/MgO nanofiber membranes by using electrospinning and employed PVA as a sacrificial template. The membranes displayed smooth nanofiber morphology and good flexibility. Fig. 1A shows a schematic diagram of the chemical reactions occurring during the preparation of electrospinning solution. To prevent the formation of a siloxane network, TEOS was hydrolyzed at room temperature. Thereafter, magnesium nitrate hexahydrate was added, which was followed by the addition of the PVA. The cross-linked hybrid structure was realized by stirring at 60 °C. Electrospun PVA/Si–Mg nanofibers

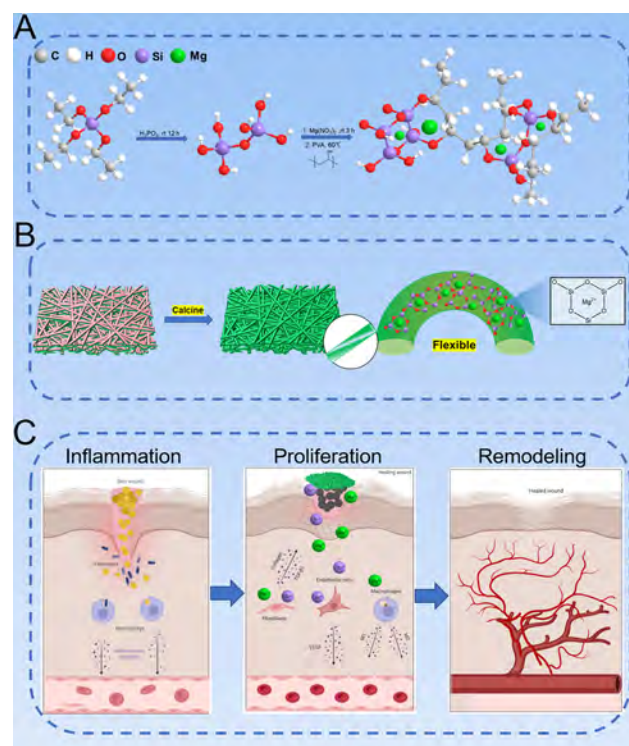


Fig. 1 (A) Synthesis scheme of precursor solutions for electrospinning. (B) Synthesis and chemical structure of flexible inorganic SiO_2/MgO nanofiber membranes. (C) Electrospun flexible SiO_2/MgO nanofiber membranes inhibit *S. aureus* infection and promote the healing process of infected wounds.

were calcined at 800 °C for 2 h to obtain a flexible SiO₂/MgO nanofiber membrane (Fig. 1B).

Generally, the SiO₂/MgO fibers are fragile which may be attributed to the crystalline grains formed during crystallization, or the low connectivity of the silica networks.^{23,24} Therefore, we assumed that the amorphous state and strong structural connectivity with high SiO₂ content could prevent the formation of cracks and fractures and endow the SiO₂/MgO nanofibers with good flexibility. By regulating the chemical composition, we were able to overcome the inherent brittle features of SiO₂/MgO nanofibers (Fig. 1B). It was found that the SiO₂/MgO-1%, SiO₂/MgO-2% and SiO₂/MgO-3% nanofiber membranes calcined at 800 °C were able to fold into complex shapes without cracking (Fig. 2A). However, the SiO₂/MgO-4% nanofiber membrane was found to be brittle and easily collapsed into small pieces after bending. SEM micrographs revealed the fibrous structure of the electrospun membranes (Fig. 2B). While nanofiber membranes exhibited similar smooth continuous nanofiber structures, they displayed different nanofiber diameters. The average fiber diameter of SiO₂/MgO-1% and SiO₂/MgO-2% membranes was slightly smaller than that of SiO₂/MgO-3% and SiO₂/MgO-4% membranes (Fig. 2F). The EDS images show the homogeneous distribution of oxygen (Fig. 2C), silicon (Fig. 2D) and magnesium (Fig. 2E) elements. The elemental density of magnesium increased gradually with an increase in the content of MgO from SiO₂/MgO-1% to SiO₂/MgO-4% membranes.

SEM images of the SiO₂/MgO-1% and SiO₂/MgO-2% nanofibers at the curved position indicate a U-shaped deflection without fracture (Fig. 3A). However, the SiO₂/MgO-3% nanofibers had only a small proportion of the fiber breakage at the bending position, and the SiO₂/MgO-4% nanofibers were completely broken once the U-shaped deflection was performed. FTIR spectra of electrospun membranes are shown in Fig. 3B. The FTIR spectrum of PVA + Si-Mg nanofiber membranes exhibited a characteristic peak of C-H stretching vibration at 954 cm⁻¹, while no corresponding characteristic peak was found in the calcined nanofiber membranes. However, in the FTIR spectrum of SiO₂/MgO membranes, peaks at 796 cm⁻¹ associated with symmetric Si-O-Si of the silica ring structures appeared. The XRD patterns of electrospun SiO₂ NF and SiO₂/MgO membranes exhibited a hump in the range of 20–30°, illustrating an amorphous state (Fig. 3C).

The SiO₂/MgO-2% and SiO₂/MgO-3% membranes showed much greater WVTRs (Fig. 3D) and water uptake ability (Fig. 3E) compared with a commercial transparent dressing (control). The WVTRs of electrospun SiO₂/MgO membranes significantly increased with an increase in the magnesium content; similarly, the water absorption capacity of the membrane also gradually became stronger. The hydrophilicity of electrospun SiO₂/MgO membranes was examined by water contact angle measurement. As shown in Fig. 3F, electrospun SiO₂/MgO membranes had contact angles in the range of 40–90°, indicating their good hydrophilicity. This finding suggests that the presence of magnesium ions in the electrospun membrane can enhance the hydrophilicity of the membrane. The SiO₂/MgO

nanofiber membranes experienced proportional weight loss over time and lost approximately 10% of their initial weight after 14 days *in vitro* (Fig. 3G). However, no significant difference was found in the weight loss of these membranes ($p = 0.9$). The release of Mg²⁺ mainly originates from the SiO₂/MgO nanofiber membranes (Fig. 3H). Specifically, magnesium ions were sustainably released from the membranes. The cumulative amount of magnesium ions released from SiO₂/MgO-2% and SiO₂/MgO-3% membranes was higher than that of SiO₂/MgO-1% ($p < 0.05$). Likewise, the release rate of silicon ions (Fig. 3I) was slow in all of the electrospun membranes. However, it should be noted that SiO₂/MgO nanofiber membranes had breaking strains of 8% which is much smaller than the skin (Fig. S1, ESI†).

3.2 Cytocompatibility and bioactivity of electrospun membranes

HUVECs and HFFs are commonly used cell lines to evaluate the cytocompatibility of scaffold materials. Live/dead staining revealed a greater proportion of live HUVECs with only a small portion of dead cells on the SiO₂/MgO-1% and SiO₂/MgO-2% membranes. In contrast, SiO₂ NF or SiO₂/MgO-3% membranes were accumulated by the greater proportion of the dead cells (Fig. 4A). Moreover, HUVECs showed greater coverage (Fig. 4B) and an elevated migratory activity upon culture with the SiO₂/MgO-2% membranes. The proliferation and cytokine production of HUVECs were found to be dose-dependent. While membranes containing a lower content of MgO increased cell proliferation (Fig. 4E) and VEGF production (Fig. 4F), the SiO₂/MgO-3% membranes significantly suppressed proliferation and VEGF production of HUVECs. Similarly, the SiO₂/MgO-2% membranes also facilitated the proliferation and cytokine production of HFFs. The HFFs exhibited a spindle shape on SiO₂/MgO membranes as revealed by live/dead staining (Fig. 4C) and SEM microscopy (Fig. 4D). The HFFs showed a greater cell area, higher portions of live cells (Fig. 4C, green staining), and increased cell coverage (Fig. 4D) on SiO₂/MgO-1% and SiO₂/MgO-2% membranes in comparison to those cells on the SiO₂ NF and SiO₂/MgO-3% membranes. Consequently, HFFs cultured on SiO₂/MgO-1% and SiO₂/MgO-2% membranes displayed an accelerated proliferation as assessed by CCK-8 assay (Fig. 4G) ($p < 0.05$). The SiO₂/MgO-2% membrane also increased ECM production showing that the fibroblasts accumulated much greater content of total protein (Fig. 4H) and collagen (Fig. 4I) ($p < 0.05$), and secreted more pro-healing transforming growth factor-beta (TGF-β1) (Fig. 4J) compared with the other membranes. Therefore, we found that the incorporation of an appropriate amount of magnesium oxide can effectively improve the biological activity of the nanofiber membrane.

Macrophages are a major cellular component of the innate immune system, which is actively involved in the wound healing process. The immune responses of these cells to biomaterials exhibit diverse plasticity ranging from pro-inflammatory to anti-inflammatory phenotypes.^{25,26} Murine macrophages exhibited a round shape with many dead cells

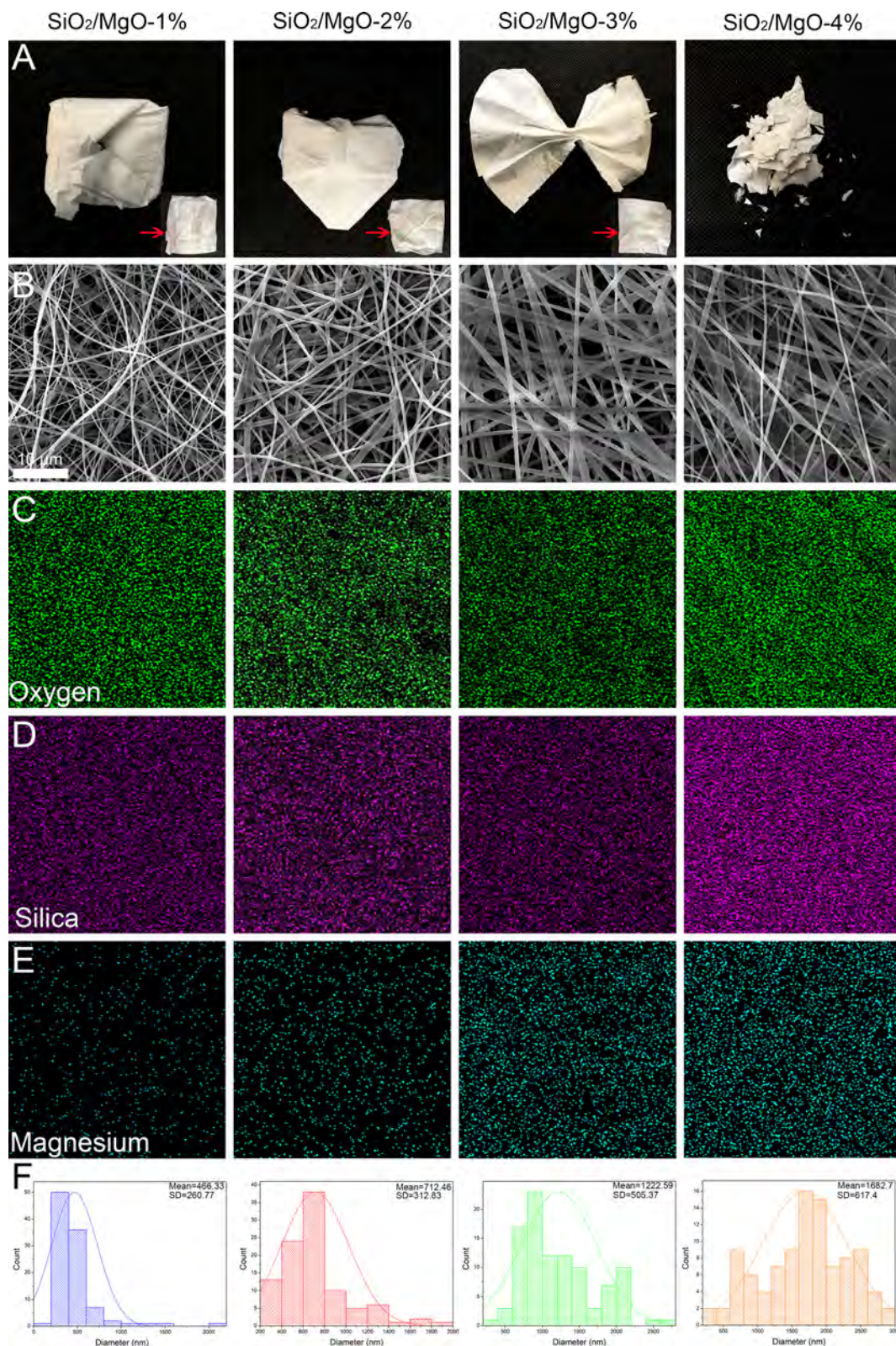


Fig. 2 Morphological analysis of flexible SiO₂/MgO membranes. (A) Photographs of flexible SiO₂/MgO-1%, SiO₂/MgO-2%, and SiO₂/MgO-3% and brittle SiO₂/MgO-4% nanofiber membranes. (B) SEM micrographs showing the nanofiber structure of electrospun membrane. Elemental mapping showing the uniform distribution of oxygen (C) and silicon (D) within electrospun membrane, while the fluorescence of magnesium (E) was increased with the amount of Mg(NO₃)₂·6H₂O incorporated in the raw material. Similarly, the nanofiber diameter (F) also increased with an increase in the content of Mg(NO₃)₂·6H₂O.

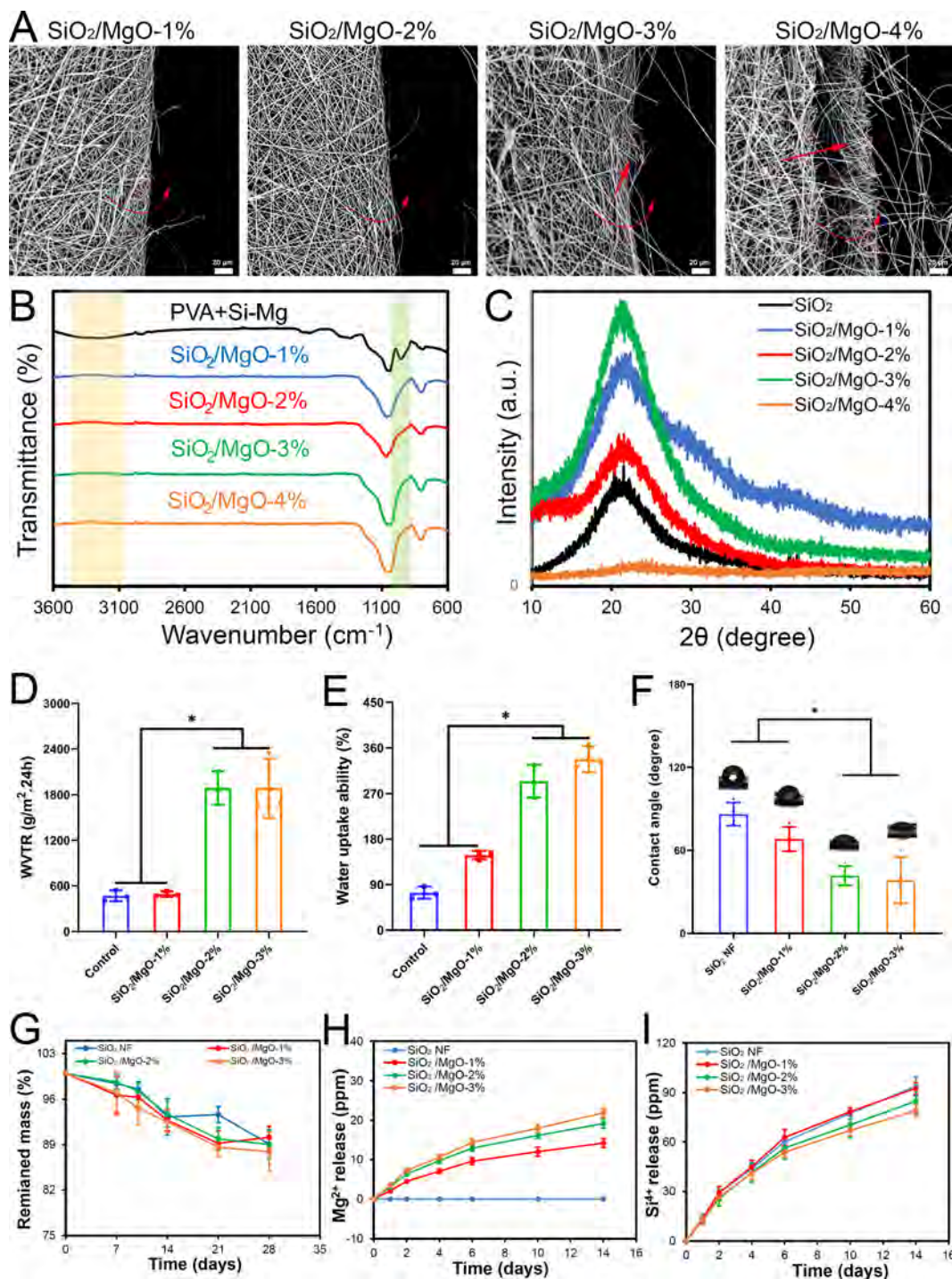


Fig. 3 Physicochemical properties of electrospun membranes. (A) SEM micrographs of the curved SiO_2/MgO membranes. The red curved arrows indicate the bending directions, while the straight arrows shown fibers breakage. The SiO_2/MgO -3% membranes have a small amount of fiber breakage, while the SiO_2/MgO -4% membranes were completely broken. (B) FTIR spectra showing the chemical structures of the electrospun membrane before and after calcination. The calcined SiO_2/MgO membranes exhibited Si–O–Si symmetrical stretching vibration of silica ring structure at 796 cm^{-1} . Similarly, the xrd patterns of nanofibers showed a hump in the range of $20\text{--}30^\circ$, indicating that the SiO_2/MgO electrospun membranes are in an amorphous state (C). The WVTRs (D) and water absorption capacity (E) of the electrospun membranes significantly increased with an increase in the magnesium content. Membranes became progressively more hydrophilic with an increase in the magnesium content (F). Degradation of membranes for up to day 28 *in vitro* (G). Membranes almost lost 10% of their weight, indicating their slow degradability. Release of magnesium ions (H) and silicon ions (I) from membranes. Statistical analysis was performed by using one-way anova with Tukey's *post hoc* test, $n = 3\text{--}4$, * indicates $p < 0.05$.

(red dots) on the SiO_2 NF membrane as revealed by live/dead staining (Fig. 5A) and SEM (Fig. 5B) images. Interestingly, both the round and spindle-shaped macrophages coexisted on SiO_2/MgO -2% membranes with much fewer dead cells (red dots).

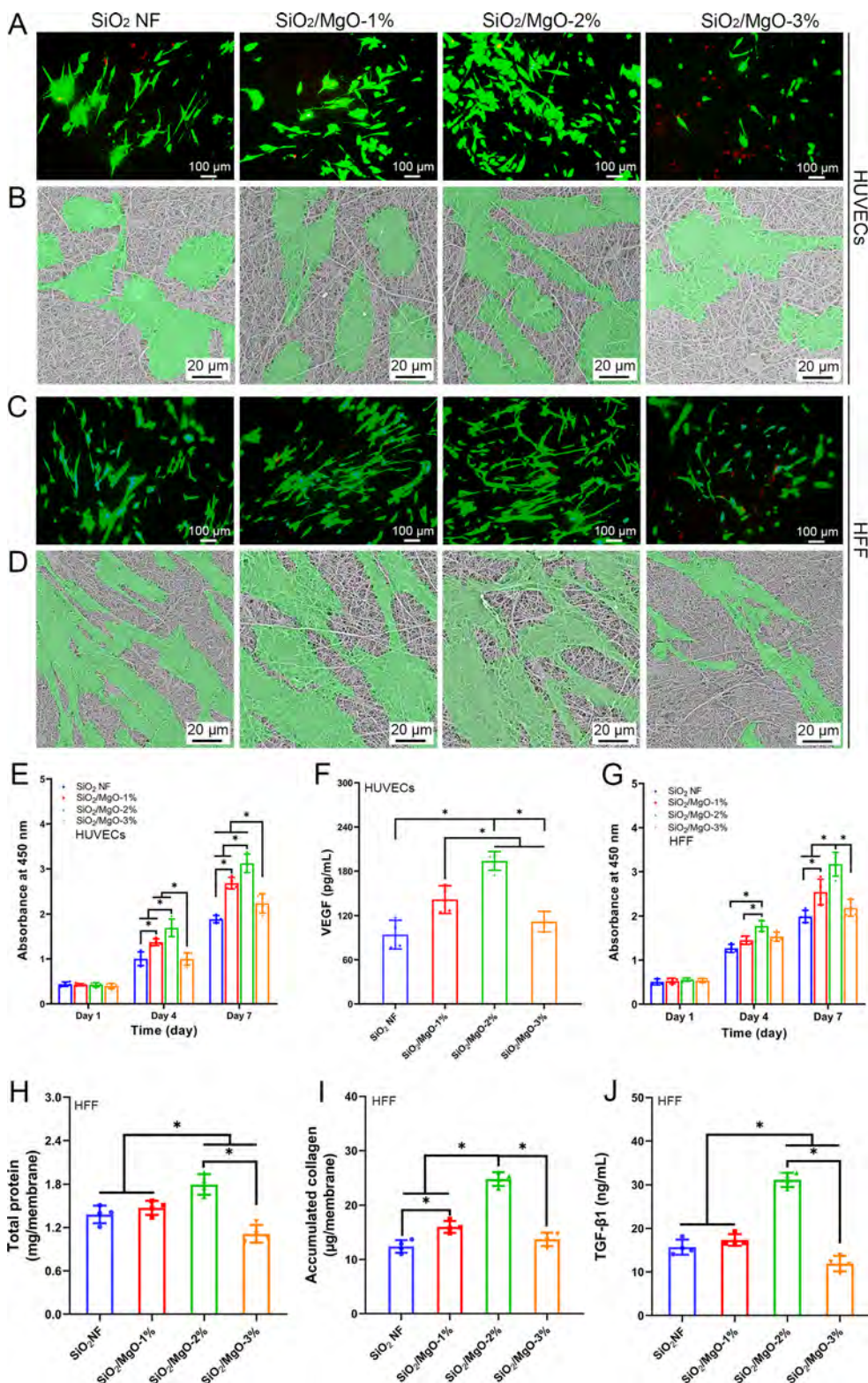


Fig. 4 Cytocompatibility and bioactivity of membranes *in vitro*. Live/dead staining (A) showed that the huvecs were predominantly viable (green) on SiO₂/MgO-1% and SiO₂/MgO-2% membranes. On the other hand, SiO₂/MgO-3% membranes exhibited greater proportion of dead cells (red). SEM micrographs (B) showed that the huvecs were well-spread with large cell area on SiO₂/MgO-1% and SiO₂/MgO-2% membranes than that of the SiO₂ nf and SiO₂/MgO-3% membranes. Similarly, live/dead assay revealed that the HFFs were of spindle-shape and exhibited higher viability on SiO₂/MgO-1% and SiO₂/MgO-2% membranes (C). The HFFs were attached and spread well on the SiO₂/MgO-2% membrane, and the cell area was larger as shown in the SEM micrographs (D). The HUVECs (E) and HFFs (F) were semi-quantitatively evaluated by cck-8 assay; SiO₂/MgO-2% membranes supported significantly higher cell proliferation rate compared to the other membranes, which further corresponded to the highest VEGF production (G), total protein deposition (H), collagen accumulation (I), and TGF-β1 secretion in these membranes than that of the other membranes (J). Statistical analysis was carried out with one-way anova with Tukey's *post hoc* test, $n = 4$, * indicates $p < 0.05$.

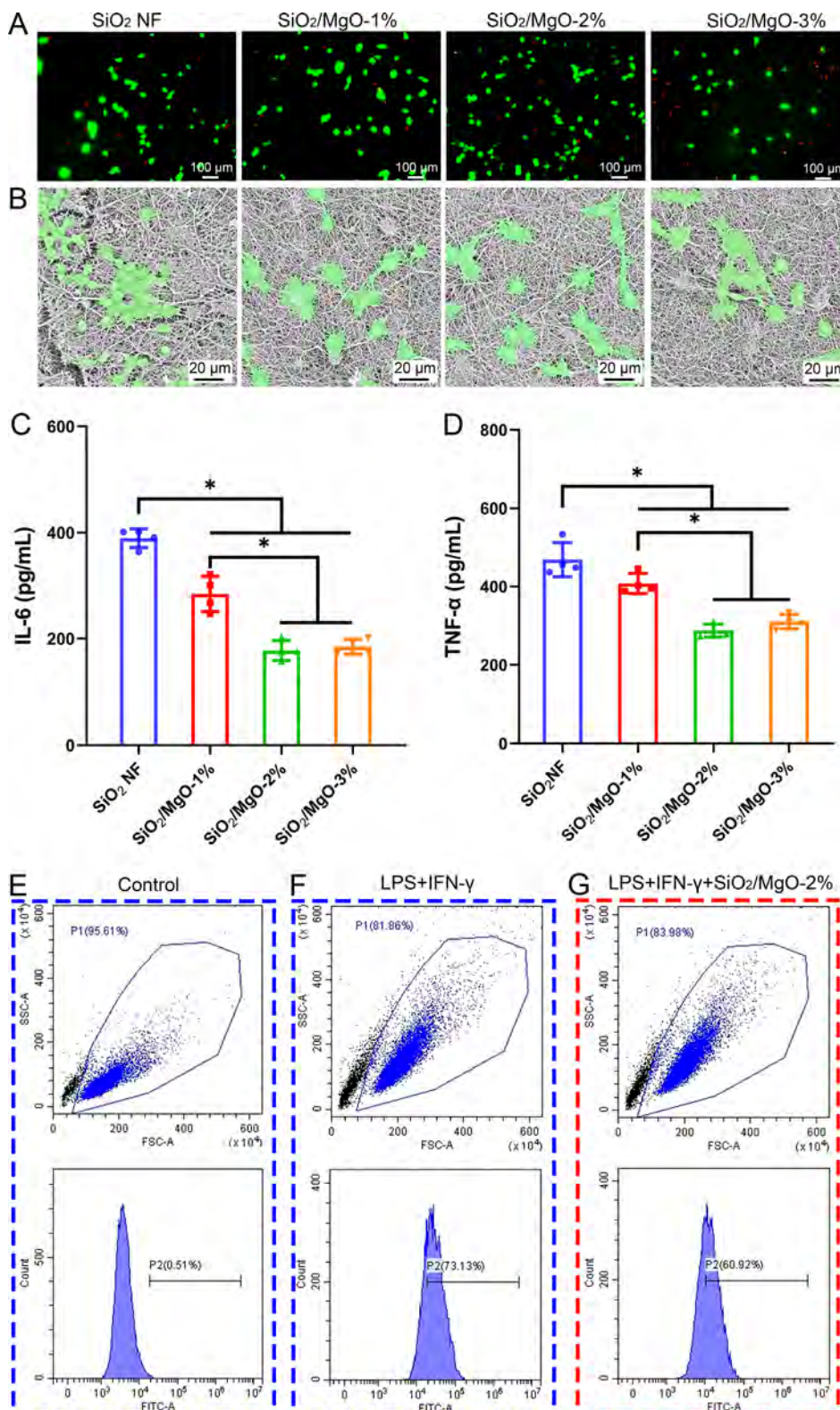


Fig. 5 The response of murine raw 264.7 macrophages to SiO₂/MgO electrospun membranes. Live/dead staining (A) shows that the SiO₂/MgO-2% membranes support more live cells (green) as compared to the other membranes. Furthermore, SEM micrographs (B) revealed that the RAW264.7 macrophages were morphologically round and more elongated on the SiO₂/MgO-2% electrospun membranes. The quantification of inflammatory factors by using ELISA, including IL-6 (C) and TNF-α (D) indicated that the SiO₂/MgO-2% membranes inhibited these factors. In addition, we used normal cultured RAW264.7 macrophages as the control group (E), and co-stimulated RAW264.7 macrophages along with lps and IFN-γ (F) and LPS + IFN-γ + SiO₂/MgO-2% group (G). Flow cytometry showed that lps and IFN-γ successfully induced the differentiation of RAW264.7 macrophages from m0 to m1 macrophages. However, SiO₂/MgO-2% membranes significantly inhibited the differentiation of RAW264.7 cells from m0 to m1 macrophages. Statistical analysis was performed by using one-way anova with Tukey's *post hoc* test, *n* = 4, * indicates *p* < 0.05.

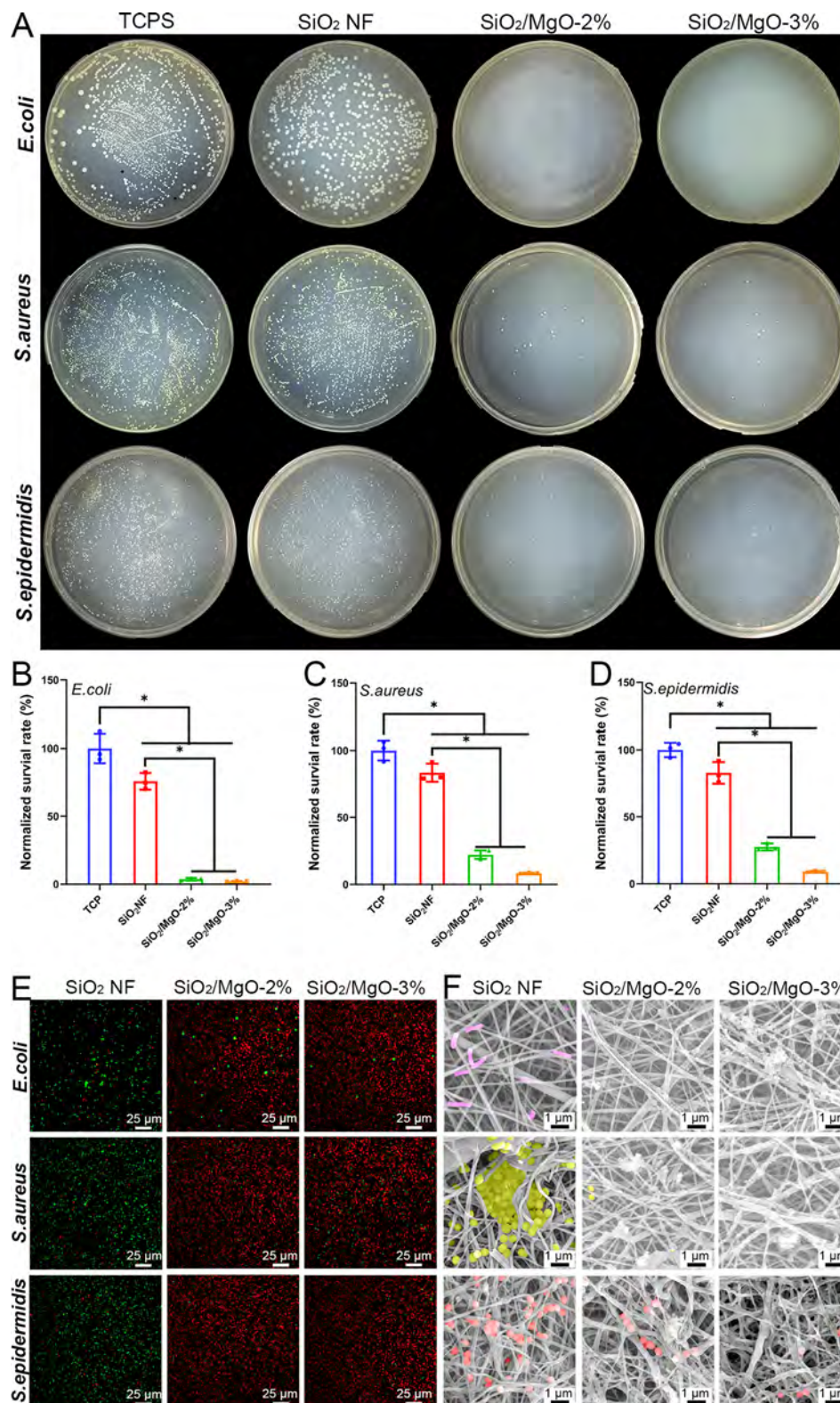


Fig. 6 *In vitro* antibacterial assay of electrospun membranes. Photographs of bacterial colonies grown on broth agar plates illustrate that *E. coli* (upper row), *S. aureus* (middle row), and *S. epidermidis* (lower row) show much fewer colonies after treating with SiO₂/MgO membranes (A). SiO₂/MgO membranes significantly reduced bacterial colonies with respect to the tcps control as well as significantly inhibited Gram-negative, *E. coli* (B) than that of the Gram-positive, *S. aureus* (C) and *S. epidermidis* (D). One-way anova with Tukey's *post hoc* test, $n = 3$, * indicates $p < 0.05$. Viability of bacteria and morphology on electrospun membranes were revealed by live/dead assay (E) and SEM (F), respectively. Bacteria showed normal morphology of rod shape (F, *E. coli*, upper row) and spherical shape (F, *S. aureus*, middle row; *S. epidermidis*, bottom row) and were predominantly survived (E, green dots) with only a few dead bacteria (E, red dots) on the SiO₂ nf membrane, while they experienced considerable cell death (E, red dots) and were broken down into debris (F) on SiO₂/MgO-2% and SiO₂/MgO-3% membranes.

In contrast, macrophages showed a spindle-shape with considerable death on the SiO₂/MgO-3% membrane. It has been shown that inflammatory responses are mainly regulated by immune cells, which is one of the important factors in the process of wound healing, and an appropriate proportion of inflammatory factors may be helpful to promote rapid wound healing.²⁷ Fig. 5C and D show the expression of IL-6 and TNF- α after co-culture of murine macrophages with different membranes. It was found that the expression of IL-6 and TNF- α in macrophages co-cultured along with SiO₂/MgO-2% and SiO₂/MgO-3% membranes was significantly lower than that of the SiO₂ NF and SiO₂/MgO-1% membranes ($p < 0.05$). It was found that the expression of IL-6 and TNF- α in macrophages on SiO₂/MgO-2% and SiO₂/MgO-3% membranes was significantly lower than that on SiO₂ NF and SiO₂/MgO-1% membranes ($p < 0.05$). The above results indicated that magnesium ions released from SiO₂/MgO nanofiber membranes could effectively inhibit the expression of IL-6 and TNF- α , which is beneficial to accelerate wound healing. To further discern the role of electrospun SiO₂/MgO-2% membranes in attenuating inflammatory responses, raw 264.7 macrophages were stimulated by LPS with IFN- γ and simultaneously co-incubated with SiO₂/MgO-2% membranes. Flow cytometry showed that the LPS combined with IFN- γ significantly induced the differentiation of M0 macrophages to the M1 macrophages (CD86-positive pro-inflammatory cells) (Fig. 5E and F), whereas co-incubation of these cells with electrospun SiO₂/MgO-2% membranes significantly attenuated M1 polarization of macrophages (Fig. 5G).

3.3 *In vitro* antibacterial activity

The antibacterial activity of electrospun SiO₂/MgO-2% and SiO₂/MgO-3% membranes against common bacterial species involved in wound infections, including *E. coli*, *S. aureus*, and *S. epidermidis* was further assessed. The antibacterial activity of electrospun SiO₂/MgO-2% and SiO₂/MgO-3% membranes was found to be dependent on the incorporation of Mg(NO₃)₂·6H₂O in the raw materials. Membranes containing higher contents of Mg showed fewer bacterial colonies (Fig. 6A) with an inhibition rate of 96%, 92%, and 90% against *E. coli* (Fig. 6B), *S. aureus* (Fig. 6C), and *S. epidermidis* (Fig. 6D), respectively. Bacterial species-maintained rod-like (*E. coli*) or spherical (*S. aureus* and *S. epidermidis*) (Fig. 6E) cell morphology with an intact surface on SiO₂ NF membranes indicating negligible effects of the SiO₂ NF membrane on bacterial survival because it only caused negligible bacterial deaths (Fig. 6E, red dots). On the other hand, SiO₂/MgO-2% and SiO₂/MgO-3% membranes containing increased amounts of Mg(NO₃)₂·6H₂O, induced considerable bacterial cell death (Fig. 6E, red dots), and the debris from the dead bacteria were found to be attached to the nanofibers (Fig. 6F).

3.4 Assessment of *S. aureus*-infected wound healing

Assessment of SiO₂/MgO membrane modulated *S. aureus*-infected wound healing was performed in an infection model of mice full-thickness skin wounds. Based on *in vitro* results, the SiO₂/MgO-2% nanofiber membrane shows good biological

activity and antibacterial properties and was therefore selected to perform the *in vivo* study. To evaluate the effect of the electrospun SiO₂/MgO-2% membrane on infected wound healing, the wound closure rate was measured by tracing the wound area at day 0, 3, 7, 10, and 14 after implantation of the membranes by using Image J software ($n = 3$ for each group). As shown in Fig. 7A, the status of wound closure in the groups treated with SiO₂/MgO-2% nearly approached the normal level as was seen in the control group (normal wounds not infected with *S. aureus*). On the other hand, SA (*S. aureus*-infected wounds) and SA + dressing groups exhibited significantly smaller wound closure rates than that of the normal control mice. In contrast, wounds treated with SA + SiO₂/MgO-2% (*S. aureus*-infected wounds) showed an accelerated healing rate as compared to the SA and SA + dressing groups. The quantitative analysis of the wound closure further shows faster wound closure in mice treated with SiO₂/MgO-2% membranes (Fig. 7B). At day 7, the percentage of wound closure in the control group (45.62% \pm 3.88%) and the SA + SiO₂/MgO-2% group (39.70% \pm 5.57%) was significantly higher than that of the SA group (20.58% \pm 5.63%) and the SA + dressing group (23.03% \pm 6.42%). At day 14, the mice exhibited almost complete wound healing in the control group (91.81% \pm 1.56%) and the SA + SiO₂/MgO-2% group (84.56% \pm 9.68%). On the other hand, wounds were largely unhealed in the SA group (48.02% \pm 14.47%) and the SA + dressing group (66.89% \pm 6.99%). These results indicate that the SA + SiO₂/MgO-2% electrospun membranes were advantageous in promoting wound healing in an infection model.

Inflammation in wounds was evaluated at gene levels using quantitative RT-PCR (Fig. 7C–J). IL-1 β , MMP-1, and TNF- α represent the major pro-inflammatory factors during wound healing. In line with evident ameliorated inflammation in wounds, the quantitative RT-PCR indicates that the SiO₂/MgO-2% membrane significantly suppressed the gene expression of IL-1 β , MMP-1, and TNF- α . Arginase-1, COL-1, IL-10, TGF- β 1, and VEGF are the major pro-healing factors during wound healing. Along with alleviated inflammatory responses, the SiO₂/MgO-2% membrane significantly up-regulated the expression levels of these pro-healing genes compared with that of the SA and SA + dressing groups.

3.5 Histological analysis

We carried out histological analysis to evaluate wound progression up to day 14 (Fig. 8A). The silicon and magnesium ions released from SiO₂/MgO-2% membranes substantially improved re-epithelialization to an extent comparable to that of the control group (normal wounds not infected with *S. aureus*). On the other hand, while the SA group lacked obvious re-epithelialization, the dressing group showed discontinuous epithelia. H&E staining further showed that the amount of granulation tissue was more abundant in the wounds treated with the SiO₂/MgO-2% membranes. In contrast, the formation of granulation tissues was significantly delayed in the SA and SA + dressing groups. The results were further confirmed by Masson's trichrome staining (Fig. 8B). Masson's trichrome staining reveals

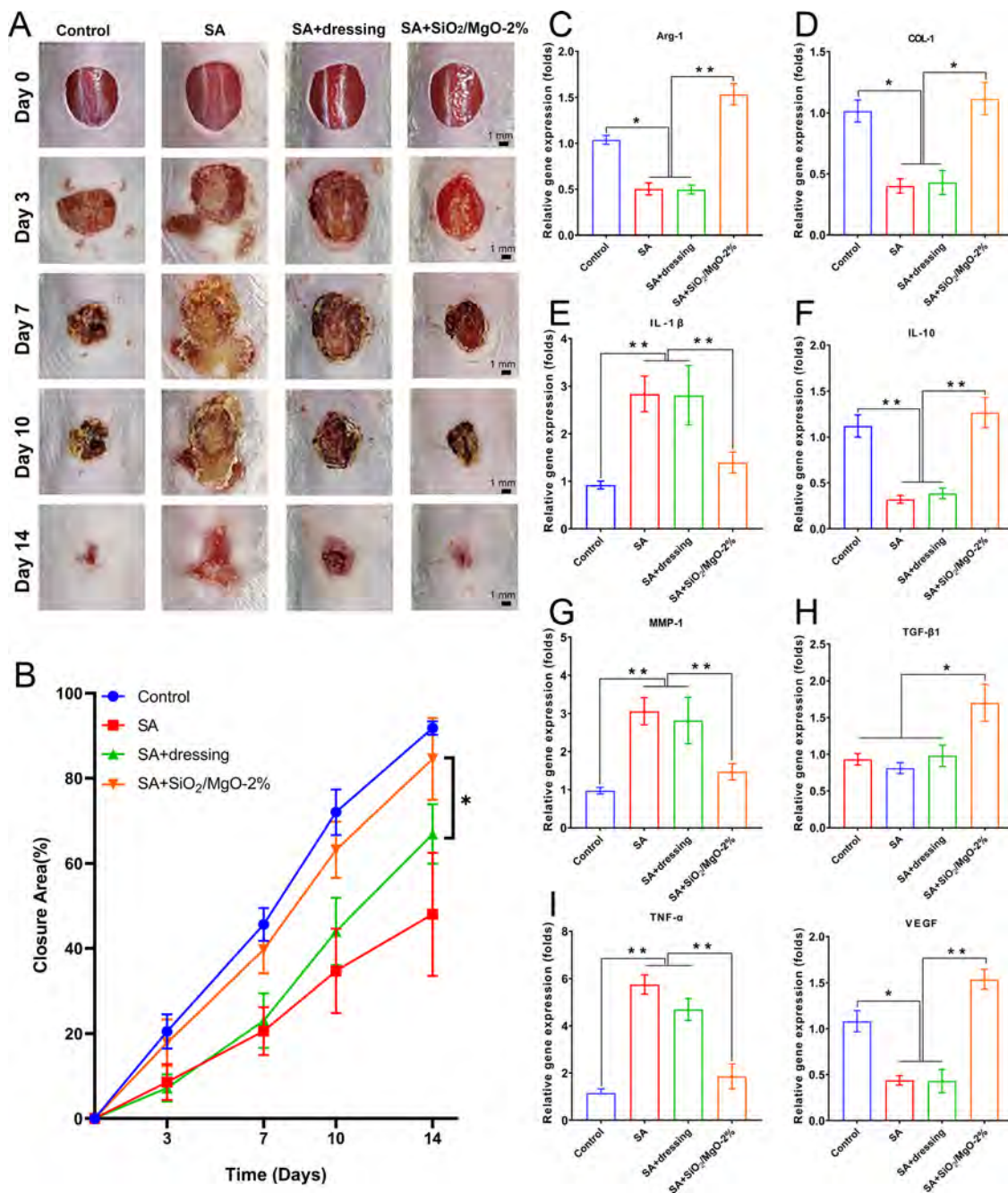


Fig. 7 *In vivo* infection model for assessing the wound healing of full-thickness defects in mice infected with *S. aureus*. Gross appearance of *S. aureus*-infected wounds treated with different dressings after 0, 3, 7, 10 and 14 days (A). The SiO₂/MgO-2% membrane effectively inhibited bacterial infection and reduced the formation of biofilm compared with wounds in the control, SA, and SA + dressing group. The wound closure curve (B) over healing time showed that the SiO₂/MgO-2% membranes significantly accelerated the healing process of *S. aureus*-infected wounds as compared to other treatments, which were almost similar to the non-infected wounds. Furthermore, RT-PCR showed significantly higher expression levels of pro-healing genes, such as Arg-1 (C), COL-1 (D), IL-10 (E) and TGF-β1 (F) in the SiO₂/MgO-2% membrane-treated wound than that of the other groups. The SiO₂/MgO-2% membranes also significantly downregulated the expression levels of pro-inflammatory cytokine genes, such as IL-1β (G), MMP-1 (H) and TNF-α (I). In addition, SiO₂/MgO-2% membrane improved the expression level of angiogenic VEGF gene (J). One-way anova with Tukey's *post hoc* test, $n = 3$, * indicates $p < 0.05$.

a large number of collagen fibers depositing in the dermal tissues in the control group by day 14, while this was slightly less in the SA + SiO₂/MgO-2% group. Only a few collagen fibers filled the wound sites in the SA and SA + dressing groups. The length of

the wound was measured and shown in Fig. 8C. There was an insignificant difference between the control group (1.8 ± 0.5 mm) and the SA + SiO₂/MgO-2% group (2 ± 0.5 mm) in terms of the length of the wound. On the other hand, the wound length was

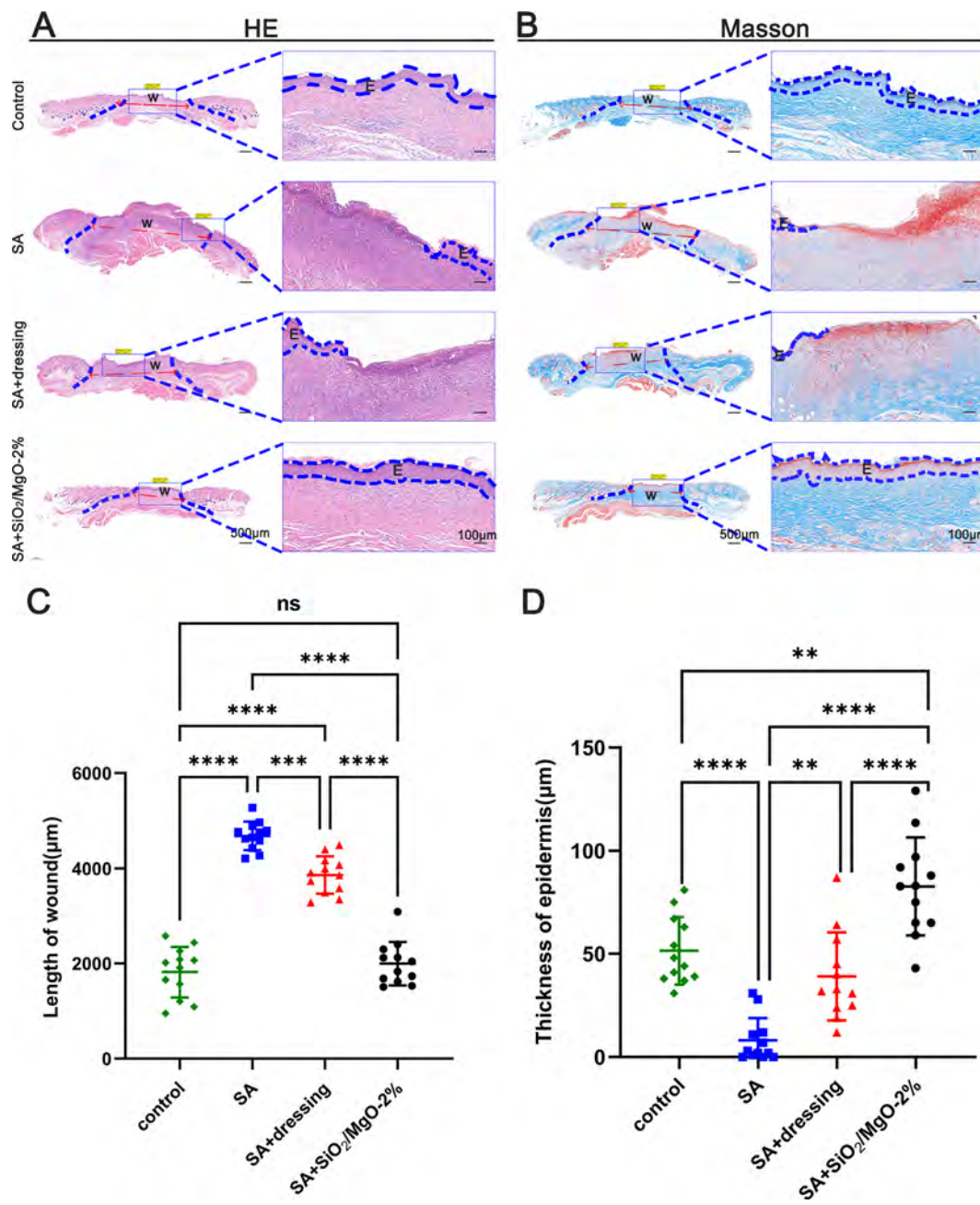


Fig. 8 Histological analysis of healed wounds by H&E (A) and masson's trichrome (B) staining. It was found (red dotted line) that the SiO₂/MgO-2% membrane could accelerate wound healing by measuring the wound length (C) on day 14. Moreover, epidermal thickness statistics (D) for wounds treated with different methods showed that (blue dotted line indicates the epithelial edge) SiO₂/MgO-2% membrane significantly accelerated epithelialization. One-way anova with Tukey's *post hoc* test, $n = 12$, * indicates $p < 0.05$.

considerably higher in the SA group (4.7 ± 0.3 mm) and the SA + dressing group (3.9 ± 0.4 mm). In addition, the thickness of the new epidermis was measured in Fig. 8D. The thickness of the neo-epidermis was also much higher in the SA + SiO₂/MgO-2% group (82.69 ± 23.81 μm) and the control group (51.50 ± 16.37 μm) than that of the SA group (8.08 ± 10.84 μm) and the SA + dressing group (39.08 ± 21.30 μm). These results indicate that SiO₂/MgO-2% membranes may significantly accelerate epithelialization and granulation tissue formation in an infected wound healing model.

3.6 Immunohistochemical analysis

At day 14, the tissues from the healed region as well as the wound edge were subjected to immunohistochemical staining by using CD31 and CD86. The wounds treated with SiO₂/MgO-2% membranes had more numbers of CD31+ blood vessels (marked by the blue arrows), whereas only a few CD31+ blood vessels were observed in the SA and dressing groups (Fig. 9A). In the healed regions, the average expression of CD86 was significantly lower in the SA + SiO₂/MgO-2% group as compared

to the SA and SA + dressing groups (marked by the blue arrows) (Fig. 9C). These results indicated that SiO₂/MgO-2% membranes significantly inhibited the infiltration of inflammatory cell types in wound areas, thus contributing remarkable wound closure. Quantitative analysis further revealed a significantly higher CD31+ vascular density in the SA + SiO₂/MgO-2% group (237.3 mm⁻²) than that of the SA group (164.8 mm⁻², $p < 0.05$) and the SA + dressing group (156.0 mm⁻², $p < 0.001$) (Fig. 9B). Similarly, the CD86 positive macrophage density was 138.2 mm⁻², 91.0 mm⁻², and 20.7 mm⁻² in the SA, SA + dressing, and SA + SiO₂/MgO-2% groups, respectively (Fig. 9D). Immunohistochemical analyses indicated that the treatment with SiO₂/MgO-2% membranes could not only increase the blood supply but also inhibit excessive inflammation in wound healing.

4. Discussion

Numerous studies have shown that electrospun nanofiber membranes incorporated with metal oxide nanoparticles exhibit great capabilities in inhibiting bacterial infection and accelerating wound healing.²⁸ For these inorganic nanoparticle-incorporated membranes, the rate at which the bioactive components are released from the nanofibers into the local environment of the lesion is critical. The rapid ion release might not be desirable for substantial tissue repair, thus necessitating controlled release strategies for wound healing.⁹ Electrospun inorganic nanofiber membranes display unique biological activities in regenerative medicine and tissue engineering applications.^{19,24} However, the inherent brittleness and

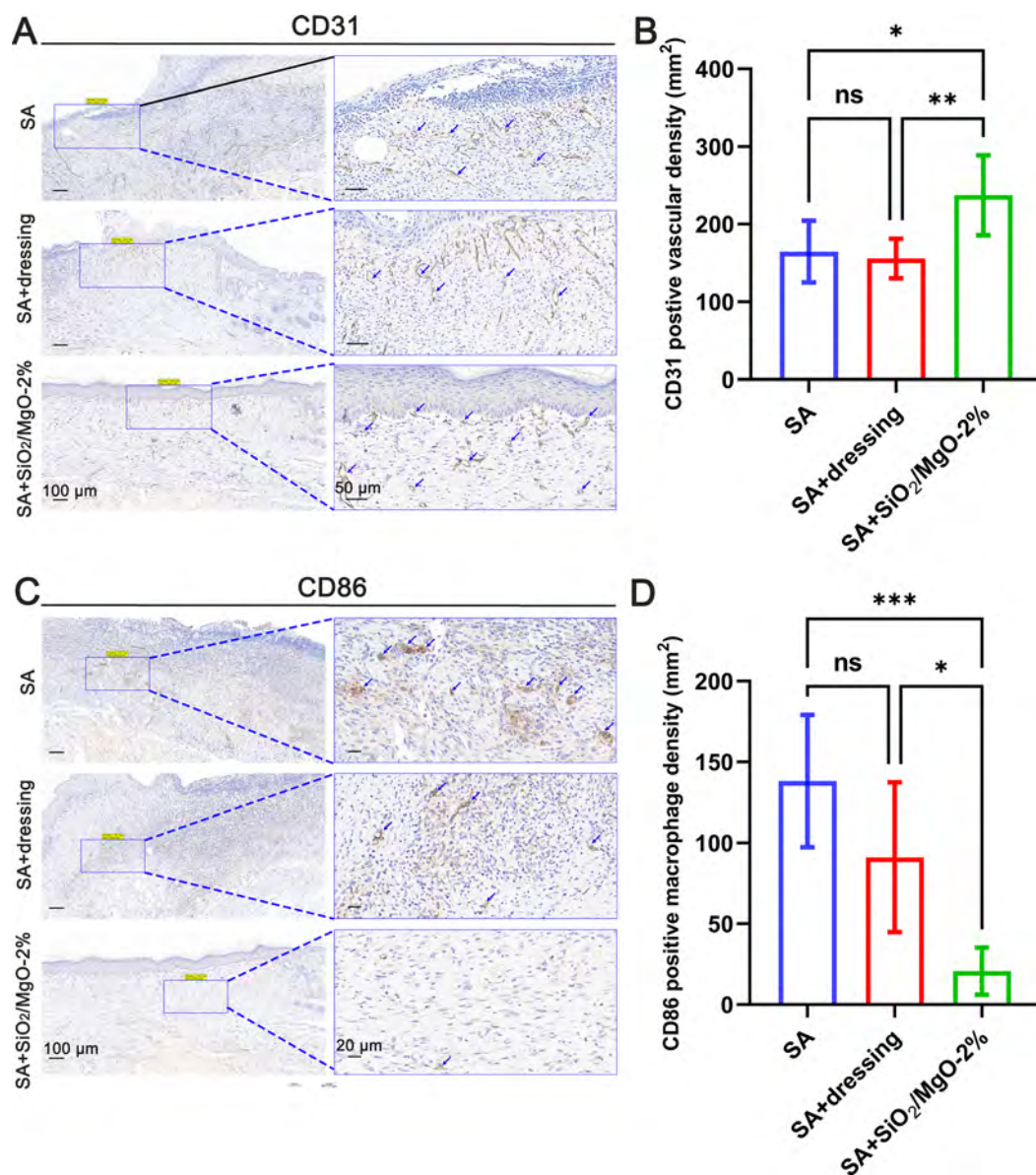


Fig. 9 Immunostaining of healed wounds at day 14. CD31+ immunohistochemical staining (A) to detect neovascularization. (B) Quantitative analysis of regenerated blood vessels. (C) Macrophages phenotypes were further elucidated by immunofluorescent staining of pro-inflammatory subpopulations (M1, CD86+). (D) Quantitative analysis of CD86. One-way anova with Tukey's *post hoc* test, $n = 6$, * indicates $p < 0.05$.

fragility of inorganic nanofibers limit their clinical applications. In this study, we reduced the brittleness of inorganic nanofibers by controlling the raw material ratio and chain structure to develop electrospun SiO₂/MgO nanofiber membranes with good flexibility and bioactivity and demonstrate their potential for wound dressing.

It is well known that the physicochemical properties including surface hydrophilicity as well as the bioactivity of nanofiber membranes affect the biological performance of wound dressings.²⁹ Since the surface hydrophilicity and release characteristics of the ions of most of the nanofiber membranes doped with inorganic nanoparticles are not optimal for biological applications, nanofiber dressings with good hydrophilicity and sustained release characteristics hold great promise. Interestingly, the water contact angle of the flexible SiO₂/MgO nanofiber membrane decreased gradually with the increasing contents of Mg(NO₃)₂·6H₂O in the raw material, indicating that magnesium improves the hydrophilicity of the obtained inorganic nanofibers. In addition, we confirmed the presence of magnesium silicate as shown by FTIR (Fig. 3B), which is generated during the calcination process.^{30–32} Magnesium silicate tremendously increases the surface wettability of SiO₂/MgO nanofiber membranes. Intriguingly, the SiO₂/MgO nanofiber membrane sustainably released Si⁴⁺ and Mg²⁺ ions over a long period *in vitro*, which indicated that the SiO₂/MgO nanofiber membrane could avoid the burst release of bioactive ions.¹¹ Most importantly, the amorphous nature and high structural connectivity encouraged the brittle-to-flexible transition of SiO₂/MgO nanofibers. Specifically, with increasing magnesium content, wollastonite crystals formed in SiO₂/MgO nanofibers. Along with the amorphous-to-crystalline transition, defects and fractures occurred, which is believed to be the main reason for the fragility of nanofibers. Additionally, the configurational transformation resulted in stronger constraints of SiO₄ tetrahedrons, which weakens the flexibility of the SiO₂/MgO backbone.¹⁹ On the one hand, SiO₂/MgO nanofiber membranes had a slow degradation profile, which make them advantageous as wound dressings. The slow degradation avoids the burst release of bioactive substances and minimizes potential toxicity to the body. On the other hand, SiO₂/MgO nanofiber membranes had small breaking strains that might limit their clinical potential for wound dressing. Future studies should focus on improving the ductility of electrospun SiO₂/MgO membranes.

The healing of skin wounds is a complex process entailing the concerted effort of various types of cells.³³ Considering the critical role of endothelial cells as well as angiogenic molecules in the wound healing process, HUVECs were co-cultured with nanofiber membranes and VEGF secretion was measured. The SiO₂/MgO-2% nanofiber membranes stimulated the angiogenesis of endothelial cells as well as induced a higher secretion of VEGF than that of the other groups (Fig. 4F). The higher VEGF production of these nanofiber membranes is ascribed to the significant release of Si⁴⁺ and Mg²⁺ ions, which may remarkably induce the angiogenesis of HUVECs *in vitro* and might also have implications to improve neovascularization at the injury

site after implantation. VEGF is the key stimulator for HUVEC proliferation, which facilitates angiogenesis and granulation tissue formation, thereby promoting re-epithelialization and wound healing.^{34,35} To verify whether SiO₂/MgO nanofiber membranes stimulated endothelial cells to secrete VEGF through released Si⁴⁺ and Mg²⁺, we performed *in vivo* studies on SiO₂/MgO-2% nanofiber membranes. Our data show that *S. aureus* infected wounds treated with SiO₂/MgO-2% membranes showed a significantly higher expression of pro-angiogenic VEGF as compared to the control, SA and SA + dressing treated wounds. Immunohistochemical analysis of SiO₂/MgO-2% treated wounds also reveals a higher expression of vascular endothelial cell marker (CD31) (Fig. 9E), further illustrating that the SiO₂/MgO-2% nanofiber membrane promoted vascularization and plays a pivotal role in wound healing. Previously, different types of growth factors have been added to wound dressings to promote angiogenesis.³⁶ However, the clinical efficacy of growth factors is limited due to their high cost and low efficiency.³⁷ In contrast, bioactive silicon and magnesium ions show several advantages, such as low cost, high stability, and improved clinical safety.^{3,21}

Collagen and anti-inflammatory factors secreted by fibroblasts are precisely regulated during the remodeling phase of wound healing, which helps to form a new connective tissue matrix.³⁸ The SiO₂/MgO-2% membrane substantially enhanced the proliferation of HFFs, extracellular matrix (ECM) production as well as the secretion of pro-healing growth factors. The amount of total collagen and TGF-β1 secreted during the co-culture of HFFs and membranes was further measured to gain an insight into the biological activities of the scaffolds (Fig. 4I–J). Notably, the SiO₂/MgO-2% group accelerated wound repair by up-regulating the production of TGF-β1 as well as improving collagen production.³⁹ These *in vitro* results were further corroborated by the *in vivo* results; SiO₂/MgO-2% membranes also up-regulated the expression of COL-1 (Fig. 7D) and TGF-β1 (Fig. 7H) genes in *S. aureus*-infected wound models in rats. We further elucidated the reparative mechanism of the SiO₂/MgO-2% membrane and found remarkable secretion of ECM as well as pro-healing growth factors, which contribute to rapid wound closure. The SiO₂/MgO-2% nanofiber membrane also promoted re-epithelialization as confirmed by the visual inspection (Fig. 7A) and histological analysis. It is therefore reasonable to infer that the SiO₂/MgO-2% membrane stimulates epidermis formation during wound healing, which leads to functional recovery of skin tissue.

Management of inflammation is critical for robust wound healing.⁴⁰ Interleukin-6 (IL-6) and tumor necrosis factor-α (TNF-α) are the major inflammatory factors.⁴¹ During wound healing, macrophages play an important role in the inflammatory phase. Our *in vitro* results revealed significantly lower levels of pro-inflammatory factors (IL-6 and TNF-α) in SiO₂/MgO-2% than that of the other groups. It is noteworthy to mention here that a direct anti-inflammatory effect of SiO₂/MgO-2% membranes cannot be assessed merely based on *in vitro* data. We therefore performed *in vivo* studies on SiO₂/MgO-2% membranes. As compared with the other three groups, the SA + SiO₂/MgO-2% group significantly down-regulated the

gene expression of pro-inflammatory factors (IL-1 β and TNF- α) while up-regulating the gene expression of anti-inflammatory factors (IL-10 and TGF- β 1). During wound healing, macrophages exhibit complex phenotypes, including M0 (not activated), M1 (pro-inflammatory), and M2 (anti-inflammatory/pro-healing), which alter with the progression of wound repair.⁴² During the inflammatory phase, macrophages mainly exhibit an M1 phenotype and express high levels of inflammatory factors, thus resulting in slow wound healing.⁴³ To verify if the SiO₂/MgO-2% membranes play a direct role in regulating inflammation by targeting macrophages, we carried out flow cytometry experiments on SiO₂/MgO-2% membranes with RAW 264.7 macrophages. The SiO₂/MgO-2% membranes significantly attenuated M1 polarization of macrophages. These *in vitro* results further corroborated the *in vivo* findings. Immunohistochemical analysis of the wound tissues revealed significantly lower expression of CD86+ macrophages (M1 phenotype) in SA + SiO₂/MgO-2% as compared to SA and SA + dressing groups (Fig. 9C), thus further showing the anti-inflammatory effect of SiO₂/MgO-2% membranes. M1 macrophages produce bactericidal inducible nitric oxide synthase (iNOS), while M2 macrophages produce arginase (Arg-1).⁴⁴ Arginase degrades arginine to ornithine, a precursor to proline, a collagen component. M2 macrophages are thought to be mainly responsible for collagen deposition/fibrosis and tissue repair.^{42,45} Therefore, we foresee that the SiO₂/MgO-2% membrane promoted wound healing by up-regulating the gene expression of Arg-1 (Fig. 7C). Matrix metalloproteinases (MMPs) are secreted by different macrophage subtypes and play an important role in wound healing.⁴⁶ However, M1 macrophages showed high expression of MMP-1. Therefore, we detected the expression of MMP-1 gene (Fig. 7G) in the wounds inoculated with *S. aureus* and treated with nanofiber membranes. The wounds treated with SiO₂/MgO-2% showed significantly lower expression of MMP-1 gene than that of the wounds treated with the SA and SA + dressing groups. Taken together, these data suggest that SiO₂/MgO-2% membranes may inhibit the expression of inflammatory factors and upregulate the expression of chemokines/growth factors (e.g., TGF- β 1, IL-10 and VEGF) through a synergistic effect of antibacterial properties and bioactivity, thereby promoting cell proliferation and vascular development; promoting fibroblasts to secrete collagen and extracellular matrix.

Bacterial infection represents one of the primary causes of wound inflammation, and *S. aureus* is the most common pathogenic bacterial species in wound infections.⁴⁷ If left untreated, wounds can sometimes develop into chronic as well as severe and life-threatening infections, thus requiring timely management of wound infections with antimicrobial wound dressings.⁴⁸ Our results showed that the SiO₂/MgO-2% membrane was highly resistant to *S. aureus* in full-thickness wounds in mice and promoted the healing process of infected wounds as fast as normal uninfected wound (control group, Fig. 7A). The SiO₂/MgO-2% membrane treated SA-infected wound (SA + SiO₂/MgO-2% group) shows a comparable healing timeline as the control group, which is much faster than the other groups (SA, SA + dressing). This promotive effect could be

attributed to its antibacterial property and good biological activity. It has been reported that the reactive oxygen species (ROS) generated by MgO were the main factors to exerting an antibacterial activity.³ Besides, magnesium and silicon ions may cause bacterial apoptosis by disrupting bacterial membranes.⁴⁹ In this study, combined with the morphology of bacterial species on the nanofiber membrane surface and the results of live/dead assay, our *in vitro* antibacterial experiments showed that the SiO₂/MgO-2% membrane contributed to the antibacterial effect (Fig. 6). At the same time, the antibacterial effect of SiO₂/MgO-2% membranes *in vivo* was obvious as revealed by the wound healing speed. Previously, we have shown that MgO-containing membranes work very well in antibacterial applications in wound management settings: MgO in membranes readily generates ROS and releases magnesium ions.⁵⁰ These factors work in concert to fight bacteria, and the SiO₂/MgO-3% nanofiber membrane with a higher content of MgO may exert a greater antibacterial activity (Fig. 6). However, after making contact with the surface of the SiO₂/MgO nanofiber membranes, the bacteria lost their structure, indicating that the MgO could destroy the cell membranes and cause the nucleic acid inside to flow outward and accumulate. As for the potential sites by which SiO₂/MgO membranes target to kill bacteria, membranes and/or walls of bacteria may be vulnerable to MgO-induced antibacterial cues. Because *E. coli* is distinct from *S. aureus* and *S. epidermidis* by membrane structure, the former is a typical Gram-negative bacterium with a thin peptidoglycan membrane while the latter Gram-positive bacteria have a thick peptidoglycan membrane, which explains the different sensitivities of these bacterial species to SiO₂/MgO nanofiber membranes.

5. Conclusions

The SiO₂/MgO nanofiber membranes prepared by sol-gel electrospinning show excellent flexibility that allows for 180° bending. Especially, the SiO₂/MgO-2% nanofiber membrane exhibits an ECM-like nanofiber structure, good hydrophilicity, and sufficient strength for wound dressing. It is of good bioactivity and significantly promotes cell proliferation and inhibits more than 96% of *E. coli* and 92% of *S. aureus*. The sustained release of silicon and magnesium ions from nanofiber membranes modulated the expression of inflammatory factors as well as angiogenic cues by stimulating effector cells. The SiO₂/MgO-2% nanofiber membrane significantly accelerates the healing of infected full-thickness wounds by inhibiting *S. aureus*-induced inflammation and promoting revascularization in a mouse model. Therefore, the current study demonstrates the antibacterial activity and bioactivity of flexible SiO₂/MgO membranes which might be promising biomaterials for wound dressing.

Ethics statement

All animal experiments were performed in accordance with the guidelines approved by the Animal Ethics Committee of Wuhan

University, and were conducted in accordance with institutional regulations after being reviewed and approved by the Department of Animal Care of Wuhan Medical University.

Conflicts of interest

The authors declare no competing financial interest.

Acknowledgements

This work was supported by the National Natural Science Foundation of China (31900949, 32050410286), the Science and Technology Commission of Shanghai Municipality (20S31900900, 19440741300, 20DZ2254900), the Sino German Science Foundation Research Exchange Center (M-0263), Deutsche Forschungsgemeinschaft (German Research Foundation (B. R.: RO 2511/11-1) and the combined Sino-German Mobility Programme of the National Natural Science Foundation of China (NSFC)/Deutsche Forschungsgemeinschaft (German Research Foundation (B. R.: M-0332)).

References

- S. Homaeigohar and A. R. Boccaccini, *Acta Biomater.*, 2020, **107**, 25–49.
- C. Cheng, Z. Shao and F. Vollrath, *Adv. Funct. Mater.*, 2008, **18**, 2172–2179.
- M. Liu, X. Wang, H. Li, C. Xia, Z. Liu, J. Liu, A. Yin, X. Lou, H. Wang, X. Mo and J. Wu, *J. Mater. Chem. B*, 2021, **9**, 3727–3744.
- W. Cheng, M. Wang, M. Chen, W. Niu and B. Lei, *Chem. Eng. J.*, 2020, **409**, 128140.
- Y. Xi, J. Ge, M. Wang, M. Chen and B. Lei, *ACS Nano*, 2020, **14**, 2904–2916.
- C. M. Desmet, V. Pr eat and B. Gallez, *Adv. Drug Delivery Rev.*, 2018, DOI: [10.1016/j.addr.2018.02.001](https://doi.org/10.1016/j.addr.2018.02.001).
- Y. Niu, Q. Li, Y. Ding, L. Dong and C. Wang, *Adv. Drug Delivery Rev.*, 2019, **146**, 190–208.
- Z. Fan, B. Liu, J. Wang, S. Zhang, Q. Lin, P. Gong, L. Ma and S. Yang, *Adv. Funct. Mater.*, 2014, **24**, 3933–3943.
- M. Liu, R. Wang, J. Liu, W. Zhang, Z. Liu, X. Lou, H. Nie, H. Wang, X. Mo, A. I. Abd-Elhamid, R. Zheng and J. Wu, *Mater. Sci. Eng., C*, 2021, 112609, DOI: [10.1016/j.msec.2021.112609](https://doi.org/10.1016/j.msec.2021.112609).
- S. Zhang, Y. Huang, X. Yang, F. Mei, Q. Ma, G. Chen, S. Ryu and X. Deng, *J. Biomed. Mater. Res., Part A*, 2009, **90a**, 671–679.
- J. Li, D. Zhai, F. Lv, Q. Yu, H. Ma, J. Yin, Z. Yi, M. Liu, J. Chang and C. Wu, *Acta Biomater.*, 2016, 254–266, DOI: [10.1016/j.actbio.2016.03.011](https://doi.org/10.1016/j.actbio.2016.03.011).
- A. A. Gorustovich, J. A. Roether and A. R. Boccaccini, *Tissue Eng., Part B*, 2010, **16**, 199–207.
- A. Hoppe, N. S. G ldal and A. R. Boccaccini, *Biomaterials*, 2011, **32**, 2757–2774.
- G. Lutz-Christian and A. R. Boccaccini, *Materials*, 2010, **3**, 3867–3910.
- R. M. Day, *Tissue Eng.*, 2005, **11**, 768.
- A. Leu and J. K. Leach, *Pharm. Res.*, 2008, **25**, 1222–1229.
- A. Leu, S. M. Stieger, P. Dayton, K. W. Ferrara and J. K. Leach, *Tissue Eng., Part A*, 2008, **15**, 877–885.
- H. Keshaw, A. Forbes and R. M. Day, *Biomaterials*, 2005, **26**, 4171–4179.
- L. Wang, Y. Qiu, Y. Guo, Y. Si, L. Liu, J. Cao, J. Yu, X. Li, Q. Zhang and B. Ding, *Nano Lett.*, 2019, **19**, 9112–9120.
- L. Wang, Y. Qiu, H. Lv, Y. Si, L. Liu, Q. Zhang, J. Cao, J. Yu, X. Li and B. Ding, *Adv. Funct. Mater.*, 2019, **29**, 1901407.
- M. Liu, M. Shafiq, B. Sun, J. Wu, W. Wang, M. El-Newehy, H. El-Hamshary, Y. Morsi, O. Ali, A. U. R. Khan and X. Mo, *Adv. Healthcare Mater.*, 2022, e2200499.
- P. Xu, Y. Xin, Z. Zhang, X. Zou, K. Xue, H. Zhang, W. Zhang and K. Liu, *BioMed Cent.*, 2020, **11**, 264.
- E. Khalil, F. H. Elbatal, Y. M. Hamdy, H. M. Zidan, M. S. Aziz and A. M. Abdelghany, *Phys. B*, 2010, **405**, 1294–1300.
- X. Song, W. Liu, S. Xu, J. Wang, B. Liu, Q. Cai, S. Tang and Y. Ma, *J. Eur. Ceram. Soc.*, 2017, **28**, 201–210.
- M. Sinha, M. Abas, S. Roy, A. Das and S. Chaffee, *Am. J. Pathol.*, 2015, **185**, 2596–2606.
- P. Luca, G. Elisabetta, B. Denisa, T. Marco, F. Matteo, B. Barbara, F. Giampietro, B. Antonino and M. Lorenzo, *J. Immunol. Res.*, 2018, **2018**, 1–25.
- T. Poonam, S. Madhuri, K. Himani, K. Anita, M. Kasturi and Z. Dongsheng, *PLoS One*, 2015, **10**, e0121313.
- X. Wang, F. Lv, T. Li, Y. Han, Z. Yi, M. Liu, J. Chang and C. Wu, *ACS Nano*, 2017, 11337–11349.
- L. Bacakova, E. Filova, M. Parizek, T. Ruml and V. Svorcik, *Biotechnol. Adv.*, 2011, **29**, 739–767.
- R. Choudhary, S. Koppala and S. Swamiappan, *J. Asian Ceram. Soc.*, 2015, **3**, 173–177.
- M. Shafiq and T. Yasin, *Radiat. Phys. Chem.*, 2012, **81**, 52–56.
- I. Ahmad, M. Shafiq and T. Yasin, *J. Appl. Polym. Sci.*, 2013, **128**, 2236–2241.
- P. Martin, *Science*, 1997, **276**, 75–81.
- A. Y. S. Law and C. K. C. Wong, *Mol. Cell. Endocrinol.*, 2013, **374**, 73–81.
- H. S. Yang, J. Shin, S. H. Bhang, J. Y. Shin, J. Park, G. I. Im, C. S. Kim and B. S. Kim, *Exp. Mol. Med.*, 2011, **43**, 622–629.
- S. Matsumoto, R. Tanaka, K. Okada, K. Arita, H. Hyakusoku, M. Miyamoto, Y. Tabata and H. Mizuno, *Plast. Reconstr. Surg. Glob. Open*, 2013, **1**, e44.
- C. T. Laurencin, K. M. Ashe, N. Henry, H. M. Kan and W. H. Lo, *Drug Discovery Today*, 2014, **19**, 794–800.
- C. Gong, Q. Wu, Y. Wang, D. Zhang and Z. Qian, *Biomaterials*, 2013, **34**, 6377–6387.
- X. Zhao, R. Dong, B. Gu and P. X. Ma, *ACS Appl. Mater. Interfaces*, 2017, **9**, 29595–29611.
- G. Chen, Y. Yu, X. Wu, G. Wang, J. Ren and Y. Zhao, *Adv. Funct. Mater.*, 2018, **28**, 1801381–1801386.
- A. Fl, A. Xl, W. B. Lin, A. Xy, A. Dm, A. Zl and A. Xl, *Int. J. Biol. Macromol.*, 2020, **149**, 627–638.

- 42 J. M. Daley, S. K. Brancato, A. A. Thomay, J. S. Reichner and J. E. Albina, *J. Leukocyte Biol.*, 2010, **87**, 59–67.
- 43 P. Lou, S. Liu, X. Xu, C. Pan and J. Liu, *Acta Biomater.*, 2020, **119**, 42–56.
- 44 J. M. Daley, S. K. Brancato, A. A. Thomay, J. S. Reichner and J. E. Albina, *J. Leukocyte Biol.*, 2010, **87**, 59–67.
- 45 S. Brancato and J. Albina, *Yearb. Surg.*, 2011, **2011**, 210–211.
- 46 T. Roch, O. Akymenko, A. Krüger, F. Jung and A. Lendlein, *Clin. Hemorheol. Microcirc.*, 2014, **58**, 147–158.
- 47 Z. A. He, H. A. Jie, L. A. Yan, A. Xi, A. Hz, A. Hw, A. Yx, W. B. Chao, W. A. Jian and L. B. Zhuang, *Biomaterials*, 2020, **258**, 120286.
- 48 Y. K. Wu, N. C. Cheng and C. M. Cheng, *Trends Biotechnol.*, 2019, **37**, 505–517.
- 49 D. A. Robinson, R. W. Griffith, D. Shechtman, R. B. Evans and M. G. Conzemius, *Acta Biomater.*, 2010, **6**, 1869–1877.
- 50 J. Sawai, H. Kojima, H. Igarashi, A. Hashimoto, S. Shoji, T. Sawaki, A. Hakoda, E. Kawada, T. Kokugan and M. Shimizu, *World J. Microbiol. Biotechnol.*, 2000, **16**, 187–194.